Vision Research 51 (2011) 2110–2120

Contents lists available at SciVerse ScienceDirect

Vision Research

journal homepage: www.elsevier.com/locate/visres

Distinct cortical responses to 2D figures defined by motion contrast

Jeremy D. Fesi [a,*], Michael P. Yannes [a], Danielle D. Brinckman [a], Anthony M. Norcia [c], Justin M. Ales [c], Rick O. Gilmore [a,b]

[a] The Pennsylvania State University, Department of Psychology, 111 Moore Building, University Park, PA 16802, United States
[b] The Penn State Social, Life, & Engineering Sciences Imaging Center, Chandlee Laboratory, University Park, PA 16802, United States
[c] Department of Psychology, Stanford University, Stanford, CA 94305, United States

ARTICLE INFO

Article history:
Received 17 January 2011
Received in revised form 15 July 2011
Available online 26 July 2011

Keywords:
Electrophysiology
Evoked potentials
Figure segmentation
Motion processing

ABSTRACT

Motion contrast contributes to the segregation of a two-dimensional figure from its background, yet many questions remain about its neural mechanisms. We measured steady-state visual evoked potential (SSVEP) responses to moving dot displays in which figure regions emerged from and disappeared into the background at a specific temporal frequency (1.2 Hz, F1), based on regional differences of dot direction and global direction coherence. The goal was to measure the cortical response function across a range of motion contrast magnitudes. In two experiments using both a low channel count electrode array (Experiment 1) and a high density array (Experiment 2), we observed two distinct phase-locked evoked responses that were similar across motion contrast type. A response at 1.2 Hz (1F1) increased in amplitude with increasing magnitudes of direction or coherence contrast. A response at 2.4 Hz (2F1) increased in amplitude, but saturated at low levels of direction or coherence contrast. The two components showed different scalp distributions – the 1F1 was strongest along medial occipital channels, while the 2F1 was bilaterally distributed. Taken together, the studies suggest that figures defined by different types of motion contrast are processed by cortical systems with similar dynamics, and that there are separable neural systems devoted to (i) signaling the absolute magnitude of motion contrast and (ii) detecting when a figure defined by motion contrast appears and disappears from view.

1. Introduction

Motion information is critical for multiple aspects of object perception. Motion contributes to the segmentation of two-dimensional figures (Canny, 1986; Gibson & Gibson, 1957; Longuet-Higgins & Prazdny, 1980; Marr & Hildreth, 1980; Regan, 1989; Regan & Beverley, 1984) when regional differences in direction and speed – or "motion contrast" (Regan & Beverley, 1984) – enable a figure to be segregated from background. Motion also contributes to the perception of the three-dimensional structure of objects (Koenderink & van Doorn, 1991; Marr & Nishihara, 1978; Marr & Vaina, 1982; Siegel & Anderson, 1988; Todd, 1984; Ullman, 1979), due in part to motion parallax (Rogers & Graham, 1979; Wallach & O'Connell, 1953). Even at the level of perceptual categorization, sparse motion information can provide salient cues to the species of a moving animal (Bellefeuille & Faubert, 1998; Mather & West, 1993; Ptito et al., 2003), and the sex and mood of human point-light walkers (Cutting, 1978; Dittrich, 1993; Dittrich et al., 1996; Kozlowski & Cutting, 1977; Mather & Murdoch, 1994; Neri, Morrone, & Burr, 1998).

Nevertheless, many questions about the contribution of motion information to object perception remain unexplored. Psychophysical studies (de Bruyn & Orban, 1999; Nawrot & Sekuler, 1990; Regan, 1989; Regan & Beverley, 1984; Regan & Hamstra, 1992a, 1992b; Segaert, Nygård, & Wagemans, 2009; Sekuler, 1990) have explored adults' sensitivity to motion contrast defined by differences in direction, speed, and dot lifetime. These studies have found that thresholds for both the detection and discrimination of motion-defined figures have parametric constraints similar to those for luminance-defined figures, which may reflect common mechanisms shared across modalities. Similar studies on infants demonstrate that the ability to detect motion-defined figures emerges early in postnatal development (Johnson & Aslin, 1998; Kaufmann-Hayoz, Kaufmann, & Stucki, 1986), and is present as early as 2 months of age (Johnson & Mason, 2002), yet detection abilities continue to develop into childhood (Giaschi & Regan, 1997; Gunn et al., 2002; Parrish et al., 2005; Schrauf, Wist, & Ehrenstein, 1999). What brain networks contribute to the processing of motion contrast and motion-defined figures in humans is not fully understood.

Electrophysiological studies in the cat (Hammond & MacKay, 1975; Kastner, Nothdurft, & Pigarev, 1997; Li et al., 2001) and non-human primates (Baumann, van der Zwan, & Peterhans,

* Corresponding author. Address: 220 Moore Building, Penn State University, University Park, PA 16802, United States.
E-mail address: jdf232@psu.edu (J.D. Fesi).

0042-6989/$ - see front matter © 2011 Elsevier Ltd. All rights reserved.
doi:10.1016/j.visres.2011.07.015

1997; Gegenfurtner, Kiper, & Fenstemaker, 1996; Lamme, van Dijk, & Spekreijse, 1993; Marcar et al., 2000; Marcar et al., 1995; Mysore et al., 2006; Peterhans & Von der Heydt, 1989; Sary, Vogels, & Orban, 1993; Von der Heydt & Peterhans, 1989; Zeki, Perry, & Bartels, 2003) have implicated several cortical areas in motion-defined figure processing, including primary visual cortex (V1) (Peterhans & Von Der Heydt, 1989; Von Der Heydt & Peterhans, 1989) and area MT (Allman, Miezin, & McGuiness, 1985; Born & Tootell, 1992; Marcar et al., 2000; Orban & Gulyas, 1988; Tanaka et al., 1986). The sensitivity of cells in macaque MT to local motion contrast, particularly due to differential stimulation of center and antagonistic surround regions, has been cited as a possible source of motion-defined figure or contour processing (Allman, Miezin, & McGuiness, 1985; Born, 2000; Born & Tootell, 1992; Gautama & van Hulle, 2001; Gegenfurtner, Kiper, & Fenstemaker, 1996; Huang, Albright, & Stoner, 2007; Orban & Gulyas, 1988; Petkov & Subramanian, 2007; Sakai & Nishimura, 2006; Tanaka et al., 1986), as well as for motion-defined surface curvature (Xiao et al., 1997a, 1997b). Other areas implicated include V2 (Baumann, van der Zwan, & Peterhans, 1997; Marcar et al., 1995), V3 and V3a (Zeki, Perry, & Bartels, 2003), and V4 (Mysore et al., 2006), all of which have demonstrated a cue-invariant sensitivity to contours or figures in certain contexts.

Human neuroimaging studies employing positron emission tomography (PET) (DuPont et al., 1997; Orban et al., 1995; Shulman et al., 1998) and functional magnetic resonance imaging (fMRI) techniques (Larsson & Heeger, 2006; Likova & Tyler, 2008; Van Oostende et al., 1997; Vinberg & Grill-Spector, 2008; Zeki, Perry, & Bartels, 2003) also implicate a network of cortical areas in motion-defined figure processing. One such area is the kinetic occipital region, or KO (DuPont et al., 1997; Orban et al., 1995; Van Oostende et al., 1997), also known as V3b (Smith et al., 1998; Zeki, Perry, & Bartels, 2003). This area is regarded by some as "specialized in the processing of kinetic contours" (DuPont et al., 1997), and by others as important for cue-invariant contour processing (Larsson & Heeger, 2006; Zeki, Perry, & Bartels, 2003) or for depth structure (Tyler et al., 2006). Other regions in human visual cortex that have been demonstrated to play a role in motion-defined figure processing include areas hMT+/V5 (Likova & Tyler, 2008), V3 and V3a (Bartels, Zeki, & Logothetis, 2008; Wattam-Bell et al., 2010; Zeki, Perry, & Bartels, 2003), and the lateral occipital complex (LOC) (Vinberg & Grill-Spector, 2008), a region with a cue-invariant sensitivity to figure information (Appelbaum et al., 2006, 2008).

These past experiments, however, provide little information about how neural responses to motion-defined figures depend on the strength or magnitude of motion contrast information or whether there is a form of cue-invariance in the processing of figures defined by different types of motion contrast. In the experiments reported here, we systematically varied the magnitude of motion contrast between figure and background. We created figures defined either by differences in uniform motion direction between figure and background or differences in the global dot direction coherence. Global coherence reflects the statistical distribution of local direction vectors (see Morgan & Ward, 1980; Newsome & Pare, 1988), and variations in coherence have been used to investigate the direction tuning of MT cells (Britten et al., 1992). Similarly, a population of cells in MT show center–surround motion opponency (e.g. Born, 2000). Accordingly, we chose to manipulate both uniform direction differences between figure and background, and figure/ground coherence differences in order to recruit area hMT+, one of the core nodes of the cortical network engaged in motion processing (Allman, Miezin, & McGuiness, 1985; Born, 2000; Born & Tootell, 1992; Eifuku & Wurtz, 1998; Gautama & Van Hulle, 2001; Huang, Albright, & Stoner, 2007; Orban & Gulyas, 1988; Petkov & Subramanian, 2007; Sakai & Nishimura, 2006; Tanaka et al., 1986).

We measured steady-state evoked potential (SSVEP) responses to displays depicting a range of motion contrast values in order to capture the tuning of cortical responsiveness to this particular form cue. The SSVEP method is well suited to capture cortical dynamics (Hoffmann, Dorn, & Bach, 1999), and has been used to simultaneously measure both local and global motion processes (Gilmore et al., 2007; Hou et al., 2009) and other cue-invariant responses in figure processing (Appelbaum et al., 2006, 2008). We predicted that the SSVEP response would increase with the magnitude of motion contrast and that the tuning curves for both motion contrast types would be similar due to motion-cue invariance.

2. Experiment 1

2.1. Methods

2.1.1. Participants

Forty-five undergraduate and graduate students (23 female, mean age = 22, range = 18–27) from a large public university participated in the study, with 15 participants in each of three display groups. All participants had normal or corrected-to-normal vision, as assessed by a brief vision screening test of binocular optotype acuity. Most students received course credit for participating in the study, while some were paid $10 for their time.

2.1.2. Display

Participants viewed random dot kinematogram displays on a monochrome Macintosh G4 monitor with an 800 × 600 pixel resolution, at a viewing distance of 60 cm, and a 28° × 28° visual angle. The displays consisted of white dots (85 cd/m^2) moving against a black screen of 0.7 cd/m^2 (mean luminance = 43 cd/m^2; luminance contrast = 90%) at a dot update rate of 36 Hz, and a screen refresh rate of 72 Hz. Dot displacement was 10 amin for all conditions, for a speed of 6°/s. For the sake of compatibility with previous studies (Gilmore et al., 2007; Hou et al., 2009), we used unlimited dot lifetimes.

The displays contained four 9° × 9° square shaped "figure" regions that emerged from and disappeared into the background at a fixed frequency of 1.2 Hz (referred to as the fundamental frequency, or F1). Each display modulated between a Figure Off phase, during which all dot motion settings were identical, and a Figure On phase, during which regional motion contrast defined the figure regions (see Fig. 1). A full display cycle consisted of 833 ms of on/off modulation, with 417 ms of Figure On and 417 ms of Figure Off. The motion contrast types chosen were differences of uniform direction or global direction coherence.

Separate groups of participants viewed one of three sets of displays. For the two direction groups, the differences between figure and background were either Δ7°, Δ20°, Δ40°, Δ68°, Δ113°, Δ180°, or Δ2°, Δ10°, Δ30°, Δ60°, Δ90°, Δ135°, respectively. For the motion coherence group, the differences between figure and background were Δ10%, Δ20%, Δ40%, Δ60%, Δ80%, and Δ100%. Two direction groups were run, in order to test a larger range of values. For all conditions across the three groups, the parameter settings for figure and background dots were identical, except for a difference of a specified magnitude of dot direction or percent global coherence. Global coherence was defined as the percentage of dots that translated with a direction range of 0° (coherent), as opposed to a range of 180° (incoherent). For conditions in the coherence group, all of the dots had the same direction mean. The figure dots translated at a direction range of 8° (100% coherent figure) in the Figure On phase, then changed to a percent coherence identical to the background dots for the Figure Off phase. The percent coherence of the background, then, was the parameter that was modified for the different conditions. For both direction groups, all

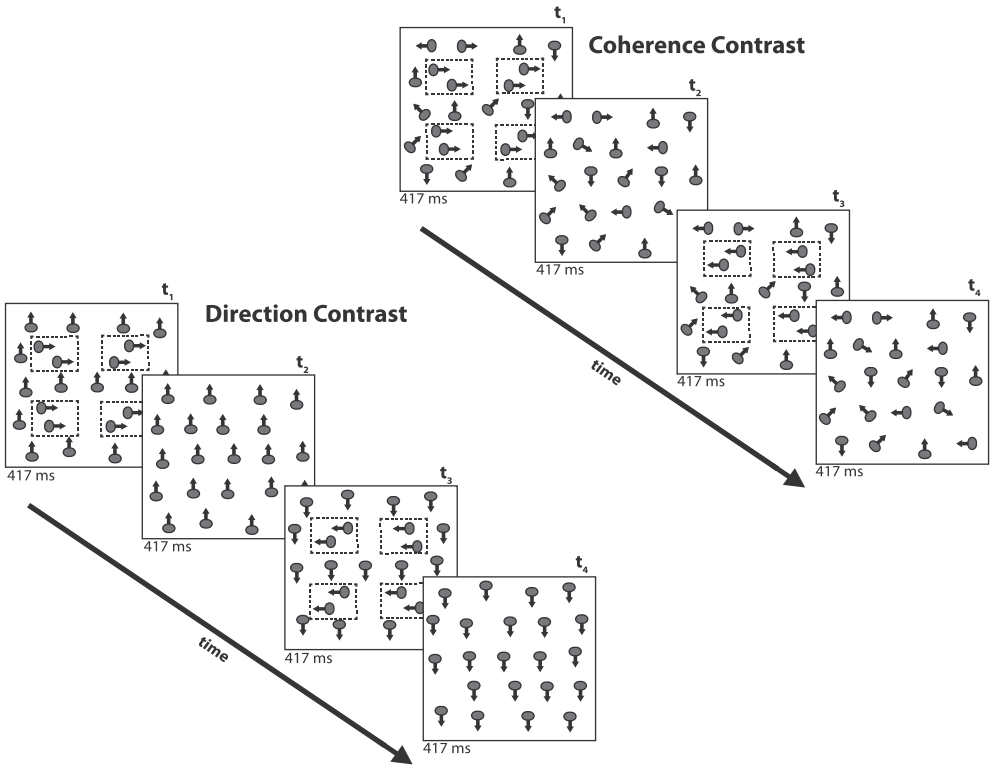

Fig. 1. Schematic representation of figure displays consisting of regional direction and coherence contrast. All displays modulated in time between a Figure On phase, in which regional contrast was present, and a Figure Off phase, in which all dot motion settings were identical. A full display consisted of 417 ms of Figure On and 417 ms of Figure Off, for a total of 833 ms per cycle. For all displays, figure and background motion reversed in direction every other cycle (0.5 Hz). The above illustration depicts two displays cycles, with direction reversal. In this sample direction contrast display, the figure dots translate 90° against the background dots in the Figure On phase. In the coherence contrast condition, 100% coherent figure dots move against background dots with 0% coherence.

dots translated at 100% coherence. The figure dots translated left and right for all conditions, and the direction of the background dots was modified for each condition.

At the start of each cycle the figures were positioned so that the innermost contours were 3° from the screen center. A white fixation cross (1.34° in diameter) was positioned at the screen center and remained in the same position throughout a trial.

2.1.3. Procedure

Participants were instructed to fixate on the cross and to try not to move or blink during trials (they were allowed to stretch and rest or close their eyes between recording trials). Each trial consisted of ten cycles of 833 ms, for a total duration of 8.33 s. Ten trials were recorded for each condition, for a total of 60 trials recorded for each of the three sessions. The typical session took 40 min to complete. To minimize adaptation, conditions were recorded in blocks of either two or four trials, mixed randomly until ten trials had been recorded for each of a session's six conditions.

2.1.4. VEP recording

Steady-state visual evoked potential (SSVEP) responses were recorded via five Grass gold cup surface electrodes placed on the scalp with a thick conductive paste (Ten-20, D.O. Weaver). The montage consisted of five points over lateral and medial occipital visual cortex, in 10–20 coordinate space: PO7, O1, Oz, O2, and PO8. All electrodes were referenced to the vertex (Cz). Electrode sites were first abraded with an exfoliating gel (NuPrep) before electrode application. Electrode impedance for each session was between 1 and 10 kΩ. The electrical activity at the scalp was amplified by a factor of 50,000 by Grass Telefactor model 15 amplifiers, with filter settings of .01–100 Hz, measured at −6 dB points. The EEG was digitized to 16 bit accuracy at a sampling rate of 432.43 Hz. Artifact rejection parameters were set to reject display cycles containing raw amplitudes that exceeded a threshold of 30 μV. If 10% of cycles within a trial were rejected, the entire trial would be rejected. Using these rejection criteria, no trials were rejected for any participant in this study. The steady-state evoked potential activity was analyzed offline with Power Diva Host software (version 2.9; Smith-Kettlewell Eye Research Institute). The software analyzes, in the frequency domain, EEG amplitudes phase-locked to the stimulus, with respect to harmonics of the modulation frequency (1.2 Hz, the fundamental frequency) of the displays, and computes a two-dimensional *t*-test called the T^2_{circ} to assess which responses are significantly above noise levels (Victor & Mast, 1991).

2.1.5. Data analysis

Linear mixed-effects modeling procedures using the *lme* command in R 2.12.2 were used to analyze the phase-locked amplitude data. We first fit an omnibus model consisting of separate within-participants factors for harmonic (1.2, 2.4, 3.6, 4.8, 6.0 Hz; 1F1, 2F1, 3F1, 4F1, 5F1; and 36 Hz, the dot update rate, 1F2), channel (PO7, O1, Oz, O2, and PO8), and motion-contrast magnitude. Then, we conducted separate analyses on the three harmonics of interest, 1F1, 2F1, and 1F2, with channel and motion-contrast magnitude as predictor variables. Linear contrasts were used to test specific differences in condition means.

2.2. Results and discussion

Fig. 2 shows a spectral plot for the responses of one participant at channel Oz, which serves as a representative illustration of the harmonics of interest for this study. Statistically significant

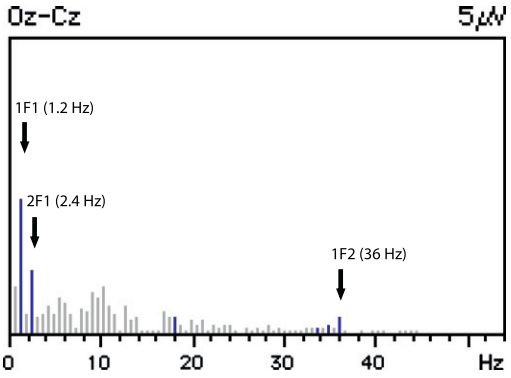

Fig. 2. Sample spectral plot of SSVEP responses for one subject at channel Oz. This highlights the harmonics of interest for this study: 1F1, 2F1, and 1F2.

phase-locked activity was observed at both the first (1F1, 1.2 Hz) and second (2F1, 2.4 Hz) harmonics of the fundamental stimulus frequency. In addition, there is a peak at the dot update rate of 36 Hz (1F2). For all three groups, each channel for each condition yielded T^2_{circ} values that were significantly different from adjacent non-signal channels at the $p < .05$ level.

Fig. 3(1) shows SSVEP amplitudes at both 1F1 (left column) and 2F1 (right column) harmonics as a function of motion contrast type (rows), motion contrast magnitude, and channel. For all three motion contrast types, 1F1 amplitudes increase monotonically as a function of motion contrast magnitude. The responses appear maximal at midline electrodes. Similar overall response patterns were seen in the two direction groups, in which different, but interleaved direction values were used.

The right column of Fig. 3 shows that responses at 2F1 increase as a function of motion contrast magnitude, but saturate at

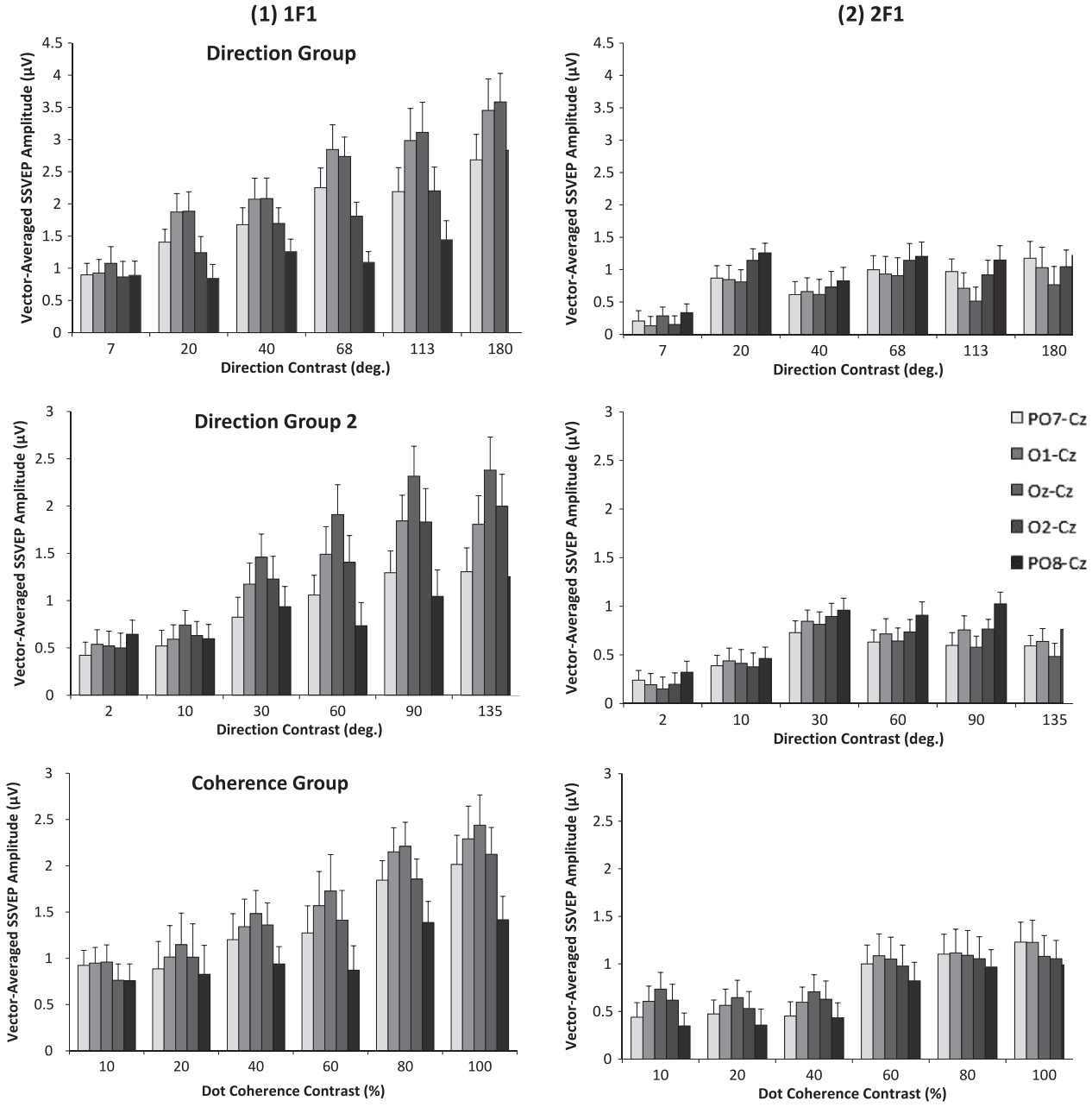

Fig. 3. SSVEP responses to figure displays defined by direction and global coherence contrast. For all three groups, responses at 1F1 (1.2 Hz) increased monotonically (1), while responses at 2F1 (2.4 Hz) increased at a specific magnitude of motion contrast, then remained invariant across subsequent increases in motion contrast magnitude (2).

relatively low levels of direction difference. The spatial distribution of responses appears larger in the lateral channels, particularly in the large (135° and 180°) direction difference conditions.

Fig. 4 shows activity at the dot update rate (1F2, 36 Hz). Statistically significant responses were observed only for medial channels. SSVEP amplitudes were much smaller than responses at 1F1 and 2F1 and appeared not to vary with the magnitude of either direction- or coherence-based motion contrast.

Separate three-way repeated measures analyses of variance (ANOVAs) with motion contrast magnitude, electrode channel, and harmonic as factors was used to quantify these effects. For direction group 1, this analysis showed significant main effects of condition, $F(5,2506) = 53.16.$, $p < .0001$), channel, $F(4,2506) = 10.98$, $p < .0001$), and harmonic, $F(5,70) = 525.77$, $p < .0001$), as well as channel-by-harmonic, $F(20,2506) = 8.66$, $p < .0001$), and condition-by-harmonic, $F(25,350) = 14.18$, $p < .0001$) interactions. A separate two-way analysis of the 1F1 responses in the direction one group showed main effects of channel $F(4,406) = 24.31$, $p < .0001$, and condition, $F(5,406) = 45.82$, $p < .0001$. Contrast tests confirmed that the medial channels (O1, Oz, and O2) had larger 1F1 amplitudes than lateral channels, $t(406) = 7.72$, $p < .0001$, and a linear pattern of amplitude increase across the set of directions, $t(406) = 8.55$, $p < .0001$. Responses at the second harmonic showed only a main effect of condition, $F(5,406) = 21.75$, $p < .0001$. Second harmonic amplitudes increased across direction contrast amplitudes, $t(406) = 4.183$, $p < .0001$, but the four highest direction levels did not differ from one another, $t(406) = .98$, n.s., confirming the saturation effect observed in Fig. 3.

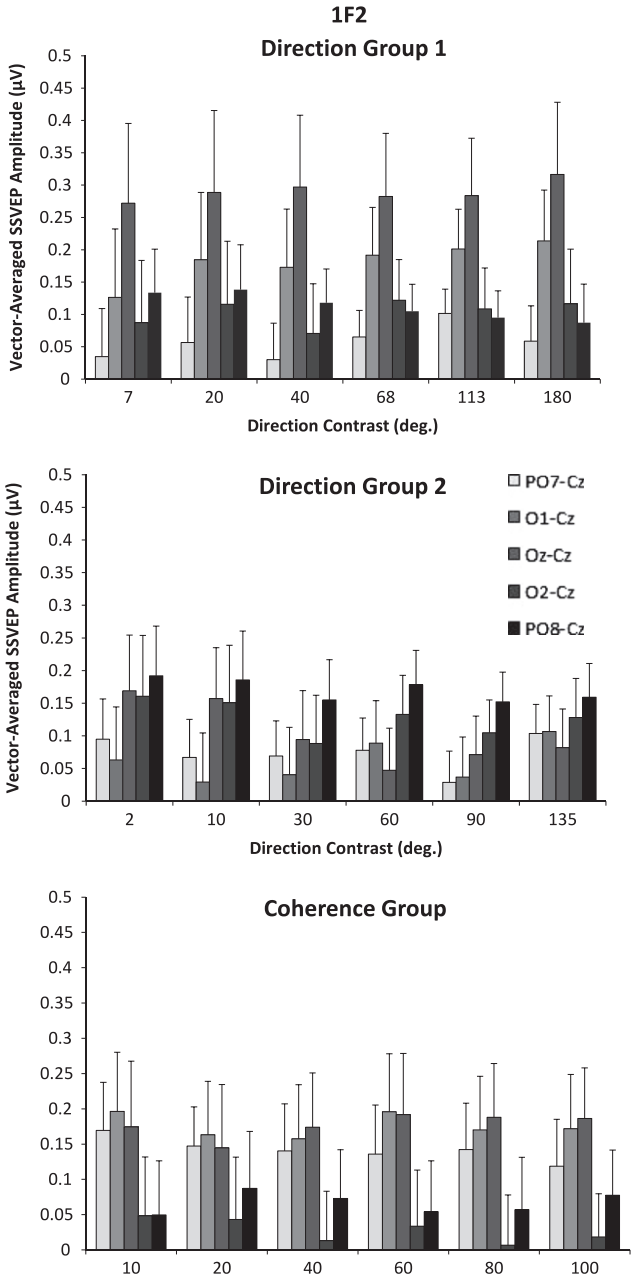

Fig. 4. Responses at 1F2 (36 Hz) were much smaller, and showed greater inter-subject variability, than the 1F1 and 2F1 responses, but significant responses were found at medial channels. Amplitudes at 1F2 were constant across magnitudes of motion contrast for all groups.

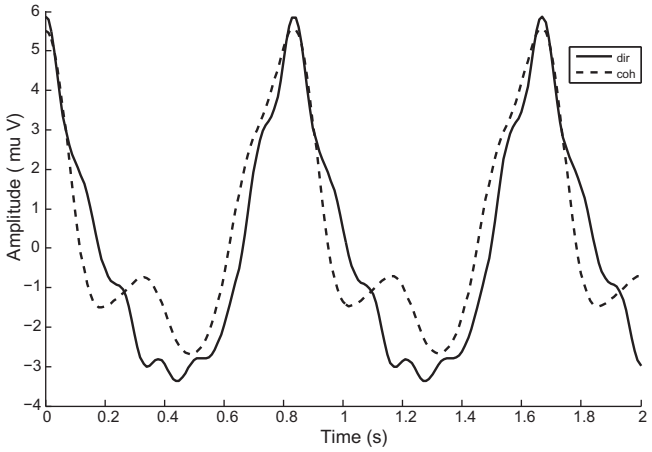

Fig. 5. Group-averaged responses across time for dot coherence (blue line) and direction (black line) contrast groups at channel Oz. The responses for the two motion contrast types are nearly identical in amplitude and phase with regard to the modulation of the displays. (For interpretation of the references to color in this figure legend, the reader is referred to the web version of this article.)

For direction group 2, the model showed effects of magnitude, $F(5,2506) = 40.54$, $p < .0001$), channel, $F(4,2506) = 9.91$, $p < .0001$), and harmonic, $F(5,2506) = 482.35$, $p < .001$) – as well as channel-by-harmonic ($F(20,2506) = 5.81$, $p < .0001$) and magnitude-by-harmonic ($F(25,2506) = 19.07$, $p < .0001$) interactions. Separate two-way analyses of the 1F1, 2F1, and 1F2 responses with channel and magnitude as predictors showed similar patterns to direction group 1. First harmonic amplitudes differed as a function of both channel and magnitude, $ps < .0001$. The channel effect was due to larger medial channel amplitudes, $p < .0001$, and a linear trend across the direction conditions, $p < .0001$. Second harmonic amplitudes also varied by channel and magnitude, $ps < .0001$. Contrast tests confirmed the effect was due to saturation at the highest four direction conditions, and higher amplitudes in lateral channel PO8 compared to the others.

The coherence condition data showed main effects of magnitude, $F(5,2506) = 74.84$, $p < .0001$, channel, $F(4,2506) = 15.74$, $p < .0001$, and harmonic, $F(5,2506) = 857.71$, $p < .0001$, and channel-by-harmonic, $F(20,2506) = 5.23$, $p < .0001$ and magnitude-by-harmonic, $F(25,2506) = 18.77$, $p < .0001$, interactions. Separate analyses of the 1F1 responses showed main effects of channel and magnitude, $ps < .0001$. As with the direction conditions, medial channel amplitudes were larger than lateral channels, $p < .0001$, and amplitudes increased linearly with motion contrast magnitude differences between figure and background, $p < .0001$. Similarly, second harmonic responses varied by channel ($p < .01$) and magnitude, $p < .0001$. Here, the medial channels showed larger amplitudes overall, $p < .01$, and there was a linear trend across motion contrast magnitude, $p < .0001$, with no evidence of saturation among the highest levels.

Fig. 5 shows time-domain group-averaged responses from the direction group 1 and coherence conditions. These were constructed by combining the mean phase-locked responses of the signal for the first nine harmonics of the fundamental frequency. Recall that every display cycle consisted of an on/off modulation of *contrast* to *no contrast* between figure and background every .833 ms. Responses to the two contrast types appear to be similar in amplitude and phase with respect to the display modulation.

As predicted, the 1F1 response increased with the magnitude of motion contrast, and responses to the two types of motion contrast appeared quite similar. Amplitudes at 2F1, however, showed a different pattern: they increased, then saturated at relatively low levels of direction or coherence contrast, showing roughly constant activation for successive increases in motion contrast magnitude. The shape of the 2F1 activity across conditions seems to reflect a response that is relatively insensitive to contrast magnitude once a certain threshold has been reached. Cells in visual cortex have been shown to respond both to the onset and offset of a particular visual "event" (Appelbaum et al., 2006, 2008; Hubel & Wiesel, 1965, 1968; Shapley & Tolhurst, 1973; Versavel, Orban, & Lagae, 1990). Accordingly, we interpret the 2F1 responses as reflecting both the onset and offset of motion contrast. The relatively consistent response pattern across contrast magnitudes likely reflects the combined activation of a population of cells that detect both the onset and offset of motion contrast. This would give rise to activation at twice the display modulation rate. The strength of such activity would not modulate with increases of motion contrast magnitude once a certain threshold had been reached. Thus, SSVEPs to motion-defined figure displays reveal two signature responses: a motion contrast-dependent response and a contrast magnitude-invariant response, which may be important for figure–ground segmentation. The responses are similar across both types of motion contrast, suggesting activation of a cue-invariant edge or figure processing mechanism, analogous to that observed previously in EEG, fMRI, and single unit studies of lateral occipital and posterior temporal cortex (Appelbaum et al., 2006, 2008; Grill-Spector et al., 1998; Sary, Vogels, & Orban, 1993; Stoner & Albright, 1992; Zeki, Perry, & Bartels, 2003). However, these particular data cannot fully address questions about the locus of motion contrast-related activity or how motion-defined edge or figure information contributes to cue invariant processing.

3. Experiment 2

Having characterized the tuning of functions of two functionally distinct cortical responses to motion-defined figure displays, we sought to understand the spatial distribution of these responses using a high-density electrode montage of 128 channels. In order to gauge the cortical sources of the responses, we generated volumetric inverse models of the VEP data, fitted to a template brain.

3.1. Method

3.1.1. Participants

Participants consisted of 29 students from a large public university (mean age: 20.6; 16 female). All had normal or corrected-to-normal vision, as assessed by a brief visual screening. Fifteen participated in the direction condition, while the other 14 participated in the coherence condition.

3.1.2. Display

The display conditions used in this experiment consisted of a subset of the direction and coherence conditions used in Experiment 1. Due to time constraints, only a few representative magnitude values of direction and coherence contrast were selected for each display group. This was done in the interest of recording several condition types per participant, while still retaining enough information to capture the pattern of activation for each display group. For the direction conditions, the contrast values were: $\Delta 5^\circ$, $\Delta 45^\circ$, and $\Delta 180^\circ$. For the coherence conditions, the contrast values were $\Delta 40\%$, $\Delta 60\%$, and $\Delta 100\%$. All parameter settings for the displays were identical to their low-density counterparts.

3.1.3. Procedure

The recording procedure was identical to those of the previous experiments, with one minor exception: participants viewed single trials of each display condition presented in random order for one trial per block. Ten trials were recorded for each of a session's three conditions, for a total of 30 trials recorded per session.

3.1.4. VEP recording

The steady-state evoked potentials were recorded via a 128-electrode dense array (SensorNet, Electrical Geodesics, Inc.). The electrodes were referenced to the vertex (Cz), and then re-referenced to the net average. EEG was collected at a 1000 Hz sampling rate, and the signal was run through a 50 Hz low pass filter. Electrode impedance for each session was at or below 50 kΩ for all electrodes. Artifact rejection parameters similar to those of the preliminary experiments were employed to reject display cycles containing raw amplitudes that exceed a threshold of 50 μV, as well as entire trials with 15% of rejected cycles. Activity was analyzed offline via Power Diva Host 2.9 software. Topographic visualizations of the data were created with mrCurrent (Smith-Kettlewell Eye Research Institute) software.

3.1.5. EEG source modeling

We conducted source analyses of the group-averaged EEG data. In order to provide anatomical coordinates, the data was analyzed using a template brain. The template used for the source modeling was constructed from the MNI305 brain (Evans et al., 1993) provided by the FreeSurfer software package (http://surfer.nmr.mgh.harvard.edu). In the template volume, sources were defined in three orthogonal orientations on an isotropic 3D grid with source spacing of 5 mm. A model set of electrodes was aligned (6 degree of freedom rigid body transform plus scaling) with this volume based on hand-labeled fiducial landmarks of the inion, nasion, vertex, and preauricular points. The forward model was calculated based on a four-shell sphere model calculated using the MNE Suite (Mosher, Leahy, & Lewis, 1999). An 11 cm radius scalp was used with the rest of the model parameters left to the default MNE Suite settings. The defaults for the four sphere radii were: 11, 10.7, 10.1 and 9.9 cm. The default conductivities for the compartments were: .33 S/m (scalp), .04 S/m (skull), 1 S/m (CSF) and .33 S/m (brain).

The inverse solution was accomplished using an L2 minimum-norm inverse (Baillet, Mosher, & Leahy, 2001; Hämäläinen et al., 1999) applied to the average data. The amount of regularization for this solution was determined using generalized cross-validation (Wahba, 1990). Signal amplitude at each source location was calculated as the quadrature sum of the amplitudes of each of the three orientations at the source location. In the frequency domain, signal-to-noise ratio (SNR) was calculated by dividing the signal amplitude by the mean of the neighboring noise frequency sidebands. Calculation of SNR was done independently for each source location.

3.2. Results

Fig. 6 shows an interpolated distribution of the responses along the scalp at 1F1, 2F1, and 1F2 for the condition with the largest motion contrast magnitude of each group. Intensity scales for the topographic maps were normalized within each condition, so as

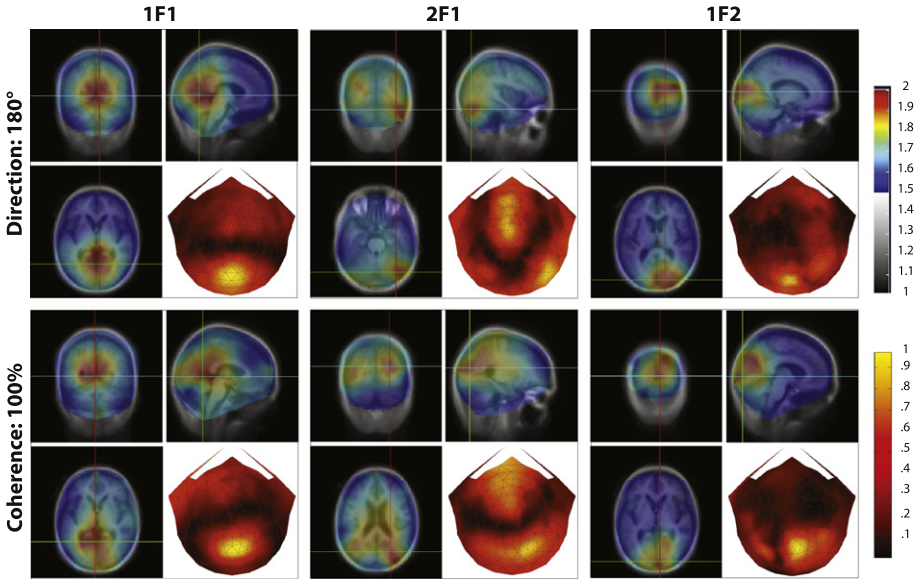

Fig. 6. SNR plots in template brain space and 2D topographic maps of SSVEP responses at 1F1, 2F1, and 1F2 to direction and coherence contrast-defined figures. All above plots correspond to the conditions of maximum motion contrast: 180° direction contrast, and 100% coherence contrast. The intensity values of the 2D scalp plots were normalized across groups and harmonics, so as to best illustrate the spatial distribution of responses at each harmonic. For both motion contrast groups, peak activity at 1F1 is medially distributed, peak activity at 2F1 is bilaterally distributed, and activity at 1F2 is also observed at medial sites, but more focally distributed than 1F1 activity.

MNI Coordinates

	Anteriormost	Posteriormost	Superiormost	Inferiormost	Leftmost	Rightmost
Dir 1F1	1, -35, -2	-19, -84, -9	1, -63.1, 29.8	1.4, -56.3, -22.8	20.9, -56.3, 6.5	-23.1, -63.1, 2.7
Dir 2F1	-41, -63.5, -22.3	-38.4, -84.8, -23.6	-36.7, -80.9, -15.1	-36.7, -76.6, -38.4	-37.5, -77.5, -27.4	-55.3, -72.9, -27.4
Dir 1F2	-0.3, -86, 4.3	0.6, -106, -17.2	-0.3, -90.2, 22.6	-0.3, -105.4, -18.9	-0.3, -87.7, 18	-40.9, -88.2, 17.5
Coh 1F1	-0.3, -30.1, 7.8	-18.9, -101.2, 9.5	-8.7, -85.1, 32.4	-9.6, -73.3, -2.4	35.3, -63.1, 1.4	-33.3, -93.3, 12.9
Coh 2F1	-35, -78.3, 12.9	-35, -99.5, 12	-35, -84.3, 25.6	-37.5, -86, 7.8	-28.2, -89.6, 12.9	-46.9, -92.4, 12.9
Coh 1F2	-5.4, -64.4, 19.2	-5.4, -92.73, 18.8	-5.4, -79.2, 18.8	-5.4, 80.9, 16.3	8.2, -83.4, 27.3	-23.1, -82,2, 26

Fig. 7. Table of MNI coordinates providing the spatial spread of the responses to maximal motion contrast at 1F1, 2F1, and 1F2.

to best illustrate the spatial spread of activation for each harmonic. For both the direction and coherence contrast groups, peak activity at 1F1 was observed across medial occipital channels, while the 2F1 responses were more widely distributed, with peak activity often observed along lateral or medial to lateral channels. Responses at 1F2 were also found among medial channels.

Fig. 6 also contains the results of a source analysis of the three harmonic responses fitted to a template brain, with coronal, axial, and sagittal views of each response. Fig. 7 provides MNI coordinates that indicate the spatial spread of the strongest signal for each response. For both motion types, 1F1 activity was observed in medial occipital cortex, extending anteriorly from early visual cortex to the lingual gyrus. Activity at 2F1 included two peaks in lateral occipital cortex: for the direction conditions, the left peak was superior to the ventrally positioned right peak; for the coherence conditions, the peaks appeared to be evenly bilateral. Responses at 1F2 were also observed in medial occipital cortex, but with a smaller spatial spread than the 1F1 responses.

Five electrode aggregate groups were created for statistical analysis and for comparison with the results of Experiment 1: medial occipital, left and right lateral, and far left and right lateral channels (see Fig. 8). The far left lateral channels were: 47, 51, 52, 58, 59, 64, and 68. The left channels were: 60, 65, 66, 67, 69, 70, and 73. The medial channels were: 71, 72, 74, 75, 76, 81, and 82. The right channels were: 77, 83, 84, 85, 88, 89, and 90. The far right channels were: 91, 92, 94, 95, 96, 97, and 98.

Separate three-way linear mixed models were again used to quantify effects of harmonic, motion contrast magnitude, and channel group. These omnibus analyses showed main effects of all three factors, *ps* < .0001, and significant condition-by-harmonic

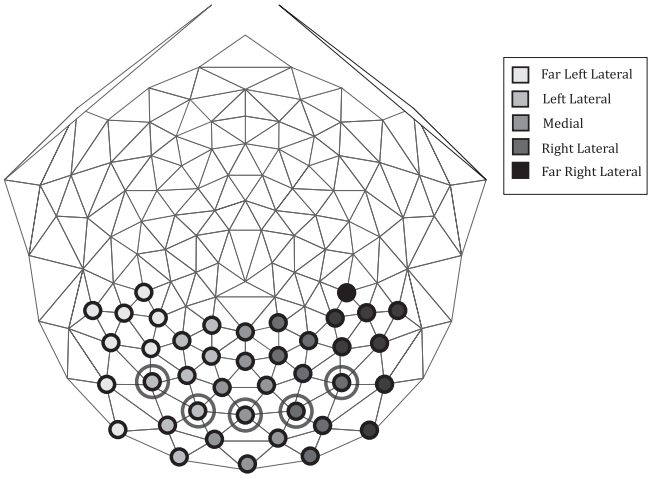

Fig. 8. Schematic representation of electrode aggregate groups chosen for analysis. Groups were chosen based on the spatial distribution of responses depicted in Fig. 5. Channels corresponding to the 10–20 electrode placement system positions used in our low-density study are indicated by surrounding ellipses.

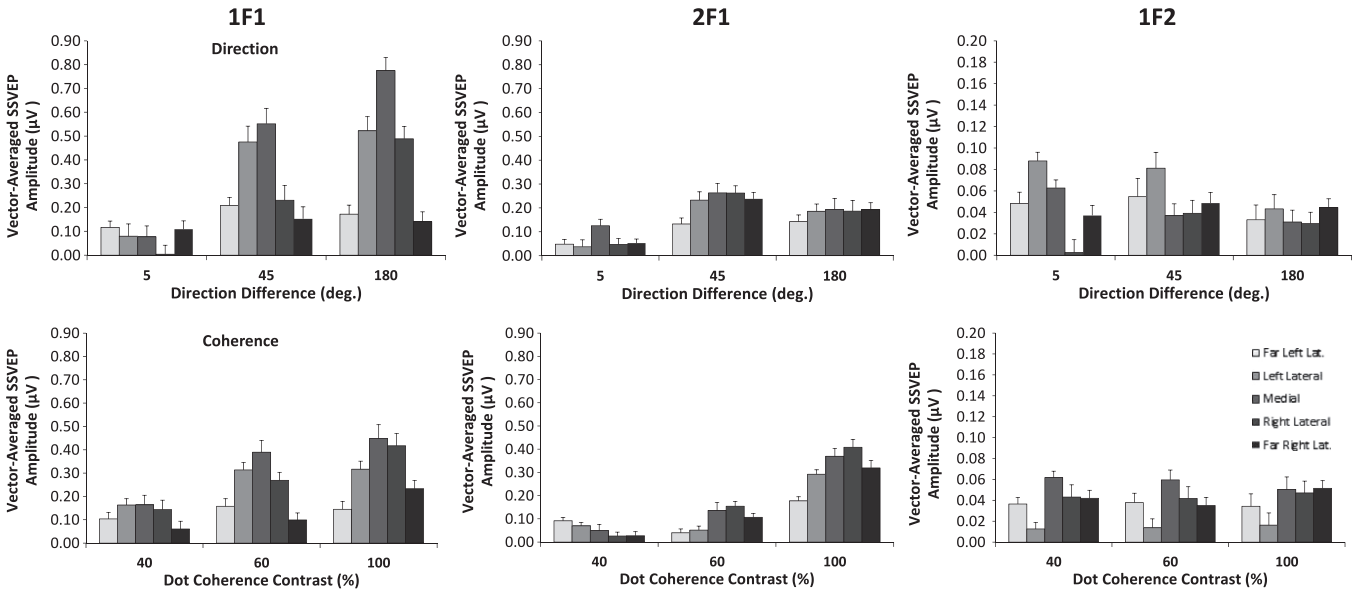

Fig. 9. SSVEP responses to figure displays defined by direction and global coherence contrast in five electrode aggregate groups. Electrodes in medial and lateral occipital regions showed response patterns that were compatible with those of our low-density experiment. Responses at 1F1 increased monotonically among medial electrodes, and responses at 2F1 that increased then saturated across subsequent increases in motion contrast magnitude were bilaterally distributed.

and channel group by harmonic interactions, $ps < .01$. Here, we report analyses on the two harmonics (1F1 and 2F1) with responses that are modulated by motion contrast magnitudes. The direction condition showed significant main effects of motion contrast magnitude, $F(2,1546) = 211.12$, $p < .0001$, and channel group, $F(4,1546) = 42.26$, $p < .0001$ and a magnitude by channel group interaction, $F(8,1546) = 7.16$, $p < .0001$, on 1F1 amplitudes. There were significant linear and (negative) quadratic trends in the 1F1 responses to motion contrast levels, $ps < .0001$, and larger responses in the medial channel group, $ps < .0001$. Second harmonic responses also varied by channel group and motion contrast magnitude, $p < .0001$, but consistent with the Fig. 6, responses were larger in lateral than midline channels, $p < .0001$. The coherence condition data were similar. First harmonic amplitudes varied as a function of motion contrast magnitude and channel, and there was also a magnitude by channel interaction, all $ps < .001$. These effects were due to a linear trend by motion contrast amplitude and larger amplitudes in the medial channels, $ps < .0001$. Second harmonic responses showed linear increases with motion contrast magnitude, $p < .0001$, but larger lateral than medial channel amplitudes, $p < .01$.

Fig. 9 illustrates the amplitudes at 1F1, 2F1, and 1F2 of electrode channels among the electrode aggregates by motion contrast condition. For both motion contrast groups, responses at 1F1 among medial electrodes increased monotonically as motion contrast magnitude increased, and responses at 2F1 across all electrode aggregate groups increased at a specific motion contrast magnitude, similar to the results of our low-density experiment. Fig. 9 shows a spatial pattern of activity that differs somewhat from the interpolated scalp distribution (Fig. 6) and our statistical analyses because the latter use phase coherent (vector) averages across the sample, which are in general more conservative measures of grouped SSVEP responses. For the plots in Fig. 9, we computed the phase coherent average within each participant and condition.

4. Discussion

We explored the tuning patterns of SSVEP responses of adult human cortex to displays of figures derived from temporal modulations of motion contrast. We compared responses to displays where figures were defined by variations in the magnitudes of dot direction or motion coherence relative to the background. The results of Experiment 1 revealed two functionally distinct cortical responses to figures specified by both types of motion contrast: one at the first harmonic of the fundamental frequency (1F1: 1.2 Hz) that increased monotonically to magnitudes of motion contrast, and another at the second harmonic (2F1: 2.4 Hz), which increased and then saturated, remaining invariant across subsequent magnitudes of motion contrast. Experiment 2 replicated the findings of Experiment 1, and provided some information about the spatial locus of SSVEP activity to motion-defined figures via a high-density electrode montage. The results demonstrated that the motion contrast-dependent response at 1F1 was strongest over medial electrode sites near the occipital pole. The 2F1 response, on the other hand, was distributed over lateral channels presumably overlying lateral occipital/posterior temporal cortex. Subsequent source localization efforts demonstrated that the 1F1 responses were strongest in medial occipital cortex, anterior to the occipital pole and extending to lingual gyrus, while the 2F1 responses peaked in lateral occipital cortex.

We interpret these findings to reflect distinct stages of motion-defined figure processing. The medially distributed response at 1F1, which is sensitive to motion contrast magnitude, may be an early process necessary for a subsequent stage of figural segmentation. The 1F1 response provides metric information about motion contrast, while the 2F1 response may be more categorical, perhaps reflecting changes in the state of segmentation. A similar metric vs. categorical distinction has been observed for binocular disparity processing with responses coding disparity magnitude being dominant in dorso-medial cortex and a categorical response to disparity sign, independent of magnitude being present in lateral cortex (Preston et al., 2008). The similarity of the 1F1 and 2F1 responses across the two types of motion contrast strengthens the argument that our displays activate cortical mechanisms with cue-invariant response properties (Appelbaum et al., 2006, 2008; Grill-Spector et al., 1998; Sary, Vogels, & Orban, 1993; Stoner & Albright, 1992; Zeki, Perry, & Bartels, 2003).

The inverse models of our VEP data suggest some likely cortical sources of the two responses. The distribution of the magnitude-

dependent motion contrast response in medial occipital cortex suggests that areas V1, V2, and V3 are the most likely sources. Single cell activity in cat and monkey striate cortex depend on the specific direction contrast between stimuli within and outside the classical receptive fields of V1 cells (Cao & Schiller, 2003; Shen, Xu, & Li, 2007; Sillito et al., 1995), and thus the 1F1 response could be generated as early as V1.

The human analog of primate MT (hMT+) is a possible source of the laterally distributed response observed at 2F1. The area has been implicated in the processing of many types of complex motion information (Born, 2000; Born & Bradley, 2005; Braddick et al., 2001; Britten & Newsome, 1998; de Jong et al., 1994; Lagae et al., 1994; Lam et al., 2000; Morrone et al., 2000; Ptito et al., 2001; Smith et al., 1998; Snowden et al., 1991; Tanaka & Saito, 1989) including motion contrast (Born & Tootell, 1992; Likova & Tyler, 2008; Shulman et al., 1998). Specifically, the center–surround opponency of MT cells has been interpreted to be important for motion-defined contour processing (Born, 2000; Gautama & Van Hulle, 2001; Huang, Albright, & Stoner, 2007; Petkov & Subramanian, 2007; Xiao et al., 1997a, 1997b). A neural model of motion-defined figure segmentation (Beck & Neumann, 2010; Raudies & Neumann, 2010) proposes feed-forward and feedback connections between V2 and hMT+ as important for initial contour segregation. The responses observed in our study appear consistent with such a model. The 2F1 response observed in our study, however, reflects neural activation that is invariant in magnitude once a threshold of motion contrast has been reached, while areas in the hMT+ complex have demonstrated differential activation properties across varied values for stimulus parameters such as dot density (Ferber, Humphrey, & Vilis, 2003, 2005; Mendola et al., 1999; Stanley & Rubin, 2003). Because the parameters explored in these previous studies, as well as the physiological signal measured, differ from those of our own investigation of cortical responses to motion-defined figures, generalization as to the response properties of hMT+ with regard to figure displays should be approached with caution. However, it may be that, although area hMT+ plays some important role in the processing of motion-defined figures, the response at 2F1 observed in our study reflects the activity of another cortical area.

The lateral occipital complex (LOC), an area characterized as important for motion-defined figure segregation processes, (Ferber, Humphrey, & Vilis, 2003, 2005; Grill-Spector, 2001; Grill-Spector et al., 1999), is another potential source of the 2F1 response. A series of combined SSVEP and MRI studies by Appelbaum et al. (2006, 2008) localized SSVEP activity corresponding to a figural modulation frequency to LOC. Moreover, the authors found that LOC activity modulates to the onset and offset of figures defined by multiple visual properties. Such cue invariance is important for a cortical detector of figural events, and this suggests that the response we observed at 2F1 to motion-defined figures may reflect a process that is not specific to motion.

4.1. Limitations of the present study

There were some limitations to the findings of our study. For instance, we explored only a fraction of the parameter space. It is possible that different dot sizes, modulation frequencies, or figure sizes would yield different response tuning curves. The similarity of the response tuning across motion contrast types also merits further investigation. The responses to direction and coherence contrast were collected via a between-groups design. A within-groups comparison, perhaps with the addition of conditions modulating other edge or figure cues, would be a stronger test of cue-invariance. Additionally, since we did not collect concurrent behavioral data, the link between physiological responses and perceptual sensitivity to motion-defined figures remains unexplored. This study is part of a larger project that assesses the development of brain responses to complex motion, and so, in the interest of maintaining compatibility with our infant sample, we chose not to contaminate our adult data with higher order decision-making responses. However, comparisons of neural tuning properties and psychophysical studies have shown general congruence of sensitivity patterns (Britten & Newsome, 1998; Britten et al., 1992; Celebrini & Newsome, 1994; Heuer & Britten, 2004; Nover, Anderson, & Deangelis, 2005; Tanaka & Saito, 1989; Shadlen et al., 1996). Past psychophysical experiments on the detection of motion-defined figures (Regan, 1989; Regan & Beverley, 1984; Regan & Hamstra, 1992a, 1992b; Segaert, Nygård, & Wagemans, 2009) can perhaps provide some behavioral context to our electrophysiological data. We should also note that while we believe the VEP responses we measured reflect figure–ground segmentation, the available evidence does not allow us to rule out the possibility that the response reflects a more general mechanism of regional motion contrast processing, rather than one that is specific to separating figures from backgrounds.

Finally, although our inverse models allowed us to discern the likely cortical sources of our VEP responses with respect to an average brain, these methods do not account for variations in shape and size of skull and brain among individuals. As such, they only provide approximations of the sources. Source modeling techniques that incorporate digitized spatial coordinates of electrodes on the scalp of each individual, as well as anatomical images of each subject's brain and skull (see Ales, Yates, & Norcia, 2010; Appelbaum et al., 2006, 2008, 2010) can account for this individual variation, and are therefore necessary to localize cortical sources more precisely.

In conclusion, the experiments described here show evidence for two distinct neural processes – one in which the local magnitude of motion contrast is computed from direction or direction coherence differences – and another which may reflect segmentation of figure from background regions. The two processes are distinguished by the harmonic that indexes them, the shape of the underlying response function, and by the spatial topography of the evoked response. The results comprise the first parametric investigation of evoked responses to motion-defined figure information in human adults, and serve as a baseline for future studies on the development of cortical response tuning patterns for the motion contrast magnitude and figure event responses. Finally, the data offer insights into the global computation of object information from motion, and emphasize that areas in the brain sometimes described as specialized for either spatial or object processing (Braddick et al., 2000; Goodale & Milner, 1992; Haxby et al., 1991; Livingstone & Hubel, 1987; Mishkin, Ungerleider, & Macko, 1983) interact extensively.

References

Ales, J. M., Yates, J. L., & Norcia, A. M. (2010). V1 is not uniquely identified by polarity reversals of responses to upper and lower visual field stimuli. *NeuroImage, 52*(4), 1401–1409.

Allman, J., Miezin, F., & McGuiness, E. (1985). Direction-and velocity-specific responses from beyond the classical receptive field in the middle temporal visual area (MT). *Perception, 14*(2), 105–126.

Appelbaum, L. G., Ales, J. M., Cottereau, B., & Norcia, A. M. (2010). Configural specificity of the lateral occipital cortex. *Neuropsychologia, 48*(11), 3323–3328.

Appelbaum, L., Wade, A., Pettet, M., Vildavski, V., & Norcia, A. (2008). Figure–ground interaction in the human visual cortex. *Journal of Vision, 8*, 1–19.

Appelbaum, L. G., Wade, A. R., Vildavski, V. Y., Pettet, M. W., & Norcia, A. M. (2006). Cue-invariant networks for figure and background processing in human visual cortex. *Journal of Neuroscience, 26*(45), 11695–11708.

Baillet, S., Mosher, J. C., & Leahy, R. M. (2001). Electromagnetic brain mapping. *IEE Signal Processing Magazine, 18*(6), 14–30.

Bartels, A., Zeki, S., & Logothetis, N. K. (2008). Natural vision reveals regional specialization to local motion and to contrast-invariant, global flow in the human brain. *Cerebral Cortex, 18*(3), 705–717.

Baumann, R., van der Zwan, R., & Peterhans, E. (1997). Figure–ground segregation at contours: A neural mechanism in the visual cortex of the alert monkey. *The European Journal of Neuroscience, 9*(6), 1290–1303.

Beck, C., & Neumann, H. (2010). Interactions of motion and form in visual cortex – A neural model. *Journal of Physiology, Paris, 104*(1–2), 61–70.

Bellefeuille, A., & Faubert, J. (1998). Independence of contour and biological-motion cues for motion-defined animal shapes. *Perception, 27*(2), 225–235.

Born, R. T. (2000). Center–surround interactions in the middle temporal visual area of the owl monkey. *Journal of Neurophysiology, 84*(5), 2658–2669.

Born, R. T., & Bradley, D. C. (2005). The structure and function of visual area MT. *Annual Review of Neuroscience, 28*, 157–189.

Born, R. T., & Tootell, R. B. (1992). Segregation of global and local motion processing in primate middle temporal visual area. *Nature, 357*, 497–499.

Braddick, O. J., O'Brien, J. M. D., Wattam-Bell, J., Atkinson, J., Hartley, T., & Turner, R. (2001). Brain areas sensitive to coherent visual motion. *Perception, 30*(1), 61–72.

Braddick, O. J., O'Brien, J. M. D., Wattam-Bell, J., Atkinson, J., & Turner, R. (2000). Form and motion coherence activate independent, but not dorsal/ventral segregated, networks in the human brain. *Current Biology, 10*(12), 731–734.

Britten, K. H., & Newsome, W. T. (1998). Tuning bandwidths for near-threshold stimuli in area MT. *Journal of Neurophysiology, 80*(2), 762–770.

Britten, K. H., Shadlen, M. N., Newsome, W. T., & Movshon, J. A. (1992). The analysis of visual motion: A comparison of neuronal and psychophysical performance. *Journal of Neuroscience, 12*(12), 4745–4765.

Canny, J. (1986). A computational approach to edge detection. *IEEE Transactions on Pattern Analysis and Machine Intelligence, 8*(6), 679–698.

Cao, A. N., & Schiller, P. H. (2003). Neural responses to relative speed in the primary visual cortex of rhesus monkey. *Visual Neuroscience, 20*(1), 77–84.

Celebrini, S., & Newsome, W. T. (1994). Neuronal and psychophysical sensitivity to motion signals in extrastriate area MST of the macaque monkey. *Journal of Neuroscience, 14*(7), 4109–4124.

Cutting, J. E. (1978). Generation of synthetic male and female walkers through manipulation of a biomechanical invariant. *Perception, 7*, 393–405.

de Bruyn, B., & Orban, G. A. (1999). What is the speed of transparent and kinetic-boundary displays? *Perception, 28*(6), 703–709.

de Jong, B. M., Shipp, S., Skidmore, B., Frackowiak, R. S., & Zeki, S. (1994). The cerebral activity related to the visual perception of forward motion in depth. *Brain, 117*(5), 1039–1054.

Dittrich, W. (1993). Action categories and the perception of biological motion. *Perception, 22*(1), 15–22.

Dittrich, W., Troscianko, T., Lea, S., & Morgan, D. (1996). Perception of emotion from dynamic point-light displays represented in dance. *Perception, 25*(6), 727–738.

Dupont, P., DeBruyn, B., Vandenberghe, R., Rosier, A., Michiels, J., Marchal, G., et al. (1997). The kinetic occipital region in human visual cortex. *Cerebral Cortex, 7*(3), 283–292.

Eifuku, S., & Wurtz, R. H. (1998). Response to motion in extrastriate area MSTl: Center–surround interactions. *Journal of Neurophysiology, 80*(1), 282–296.

Evans, A. C., Collins, S. R., Brown, E. D., Kelly, R. L., & Peters, T. M. (1993). 3D statistical neuroanatomical models from 305 MRI volumes. *IEEE, 3*, 1813–1817.

Ferber, S., Humphrey, G. K., & Vilis, T. (2003). The lateral occipital complex subserves the perceptual persistence of motion-defined groupings. *Cerebral Cortex, 13*(7), 716–721.

Ferber, S., Humphrey, G. K., & Vilis, T. (2005). Segregation and persistence of form in the lateral occipital complex. *Neuropsychologia, 43*(1), 41–51.

Gautama, T., & Van Hulle, M. M. (2001). Function of center–surround antagonism for motion in visual area MT/V5: A modeling study. *Vision Research, 41*(28), 3917–3930.

Gegenfurtner, K., Kiper, D., & Fenstemaker, S. (1996). Processing of color, form, and motion in macaque area V2. *Visual Neuroscience, 13*, 161–172.

Giaschi, D., & Regan, D. (1997). Development of motion-defined figure–ground segregation in preschool and older children, using a letter-identification task. *Optometry and Vision Science, 74*(9), 761–767.

Gibson, J. J., & Gibson, E. J. (1957). Continuous perspective transformations and the perception of rigid motion. *Journal of Experimental Psychology, 54*(2), 129–138.

Gilmore, R. O., Hou, C., Pettet, M. W., & Norcia, A. M. (2007). Development of cortical responses to optic flow. *Visual Neuroscience, 24*(6), 845–856.

Goodale, M. A., & Milner, A. D. (1992). Separate visual pathways for perception and action. *TINS, 15*(1), 20–25.

Grill-Spector, K. (2001). The lateral occipital complex and its role in object recognition. *Vision Research, 41*, 1409–1422.

Grill-Spector, K., Kushnir, T., Edelman, S., Avidan, G., Itzchak, Y., & Malach, R. (1999). Differential processing of objects under various viewing conditions in the human lateral occipital complex. *Neuron, 24*(1), 187–203.

Grill-Spector, K., Kushnir, T., Edelman, S., Itzchak, Y., & Malach, R. (1998). Cue-invariant activation in object-related areas of the human occipital lobe. *Neuron, 21*(1), 191–202.

Gunn, A., Cory, E., Atkinson, J., Braddick, O. J., Wattam-Bell, J., Guzzetta, A., et al. (2002). Dorsal and ventral stream sensitivity in normal development and hemiplegia. *Neuroreport, 13*(6), 843–847.

Hämäläinen, M., Hari, R., Ilmoniemi, R. J., Knuutila, J., & Lounasmaa, O. V. (1999). Magnetoencephalography-theory, instrumentation, and applications to noninvasive studies of the working human brain. *Review of Modern Physics, 65*(2), 413–497.

Hammond, P., & MacKay, D. M. (1975). Differential responses of cat visual cortical cells to textured stimuli. *Experimental Brain Research, 22*(4), 427–430.

Haxby, J. V., Grady, C. L., Horwitz, B., Ungerleider, L. G., Mishkin, M., Carson, R. E., et al. (1991). Dissociation of object and spatial visual processing pathways in human extrastriate cortex. *Proceedings of the National Academy of Sciences of the United States of America, 88*(5), 1621–1625.

Heuer, H. W., & Britten, K. H. (2004). Optic flow signals in extrastriate area MST: Comparison of perceptual and neuronal sensitivity. *Journal of Neurophysiology, 91*(3), 1314–1326.

Hoffmann, M. B., Dorn, T. J., & Bach, M. (1999). Time course of motion adaptation: Motion-onset visual evoked potentials and subjective estimates. *Vision Research, 39*(3), 437–444.

Hou, C., Gilmore, R. O., Pettet, M. W., & Norcia, A. M. (2009). Spatio-temporal tuning of coherent motion evoked responses in 4–6 month old infants and adults. *Vision Research, 49*(20), 2509–2517.

Huang, X., Albright, T. D., & Stoner, G. R. (2007). Adaptive surround modulation in cortical area MT. *Neuron, 53*(5), 761–770.

Hubel, D. H., & Wiesel, T. N. (1965). Receptive fields and functional architecture in two nonstriate visual areas (18 and 19) of the cat. *Journal of Neurophysiology, 28*(2), 229–289.

Hubel, D. H., & Wiesel, T. N. (1968). Receptive fields and functional architecture of monkey striate cortex. *The Journal of Physiology, 195*(1), 215–243.

Johnson, S. P., & Aslin, R. N. (1998). Young infants' perception of illusory contours in dynamic displays. *Perception, 27*(27), 341–353.

Johnson, S. P., & Mason, U. (2002). Perception of kinetic illusory contours by two-month-old infants. *Child Development, 73*, 22–34.

Kastner, S., Nothdurft, H., & Pigarev, I. (1997). Neuronal correlates of pop-out in cat striate cortex. *Vision Research, 37*(4), 371–376.

Kaufmann-Hayoz, R., Kaufmann, F., & Stucki, M. (1986). Kinetic contours in infants' visual perception. *Child Development, 57*(2), 292–299.

Koenderink, J. J., & van Doorn, A. J. (1991). Affine structure from motion. *Journal of the Optical Society of America A – Optics and Image Science, 8*(2), 377–385.

Kozlowski, L., & Cutting, J. E. (1977). Recognizing the sex of a walker from a dynamic point-light display. *Perception and Psychophysics, 21*(6), 575–580.

Lagae, L., Maes, H., Raighel, S., Xiao, D. K., & Orban, G. A. (1994). Responses of macaque STS neurons to optic flow components: A comparison of areas MT and MST. *Journal of Neurophysiology, 71*(5), 1597–1626.

Lam, K., Kaneoke, Y., Gunji, A., Yamasaki, H., Matsumoto, E., Naito, T., et al. (2000). Magnetic response of human extrastriate cortex in the detection of coherent and incoherent motion. *Neuroscience, 97*(1), 1–10.

Lamme, V. A., van Dijk, B. W., & Spekreijse, H. (1993). Contour from motion processing occurs in primary visual cortex. *Nature, 363*(6429), 541–543.

Larsson, J., & Heeger, D. (2006). Two retinotopic visual areas in human lateral occipital cortex. *Journal of Neuroscience, 26*(51), 13128–13142.

Li, B., Chen, Y., Li, B. W., Wang, L. H., & Diao, Y. C. (2001). Pattern and component motion selectivity in cortical area PMLS of the cat. *The European Journal of Neuroscience, 14*(4), 690–700.

Likova, L., & Tyler, C. W. (2008). Occipital network for figure/ground organization. *Experimental Brain Research, 189*(3), 257–267.

Livingstone, M. S., & Hubel, D. H. (1987). Psychophysical evidence for separate channels for the perception of form, color, movement, and depth. *Journal of Neuroscience, 7*(11), 3416–3468.

Longuet-Higgins, H., & Prazdny, K. (1980). The interpretation of a moving retinal image. *Proceedings of the Royal Society of London Series B – Biological Science, 208*(1173), 385–397.

Marcar, V. L., Raiguel, S. E., Xiao, D., & Orban, G. A. (2000). Processing of kinetically defined boundaries in areas V1 and V2 of the macaque monkey. *Journal of Neurophysiology, 84*(6), 2786–2798.

Marcar, V. L., Xiao, D. K., Raiguel, S. E., Maes, H., & Orban, G. A. (1995). Processing of kinetically defined boundaries in the cortical motion area MT of the macaque monkey. *Journal of Neurophysiology, 74*(3), 1258–1270.

Marr, D., & Hildreth, E. (1980). Visual information processing: The structure and creation of visual representations. *Proceedings of the Royal Society of London Series B – Biological Science, 290*(1038), 199–218.

Marr, D., & Nishihara, H. K. (1978). Representation and recognition of the spatial organization of three-dimensional shapes. *Proceedings of the Royal Society of London Series B – Biological Science, 200*(1140), 269–294.

Marr, D., & Vaina, L. M. (1982). Representation and recognition of the movement of shapes. *Proceedings of the Royal Society of London Series B – Biological Science, 214*, 501–524.

Mather, G., & Murdoch, L. (1994). Gender discrimination in biological motion displays based on dynamic cues. *Proceedings of the Royal Society Series B – Biological Science, 258*(1353), 273–279.

Mather, G., & West, S. (1993). Recognition of animal locomotion from dynamic point-light displays. *Perception, 22*(7), 759–766.

Mendola, J. D., Dale, A. M., Fischl, B., Liu, A. K., & Tootell, R. B. (1999). The representation of illusory and real contours in human cortical visual areas revealed by functional magnetic resonance imaging. *Journal of Neuroscience, 19*(19), 8560–8572.

Mishkin, M., Ungerleider, L. G., & Macko, K. A. (1983). Object vision and spatial vision: Two cortical pathways. *Trends in Neurosciences, 6*, 414–417.

Morgan, M. J., & Ward, R. (1980). Conditions for motion flow in dynamic visual noise. *Vision Research, 20*, 431–435.

Morrone, M. C., Tosetti, M., Montanaro, D., Fiorentini, A., Cioni, G., & Burr, D. C. (2000). A cortical area that responds specifically to optic flow, revealed by fMRI. *Nature Neuroscience, 3*(12), 1322–1328.

Mosher, J. C., Leahy, R. M., & Lewis, P. S. (1999). EEG and MEG: Forward solutions for inverse methods. *IEEE Transactions on Bio-Medical Engineering, 46*(3), 245–259.

Mysore, S. G., Vogels, R., Raiguel, S. E., & Orban, G. A. (2006). Processing of kinetic boundaries in macaque V4. *Journal of Neurophysiology, 1864*, 1880.

Nawrot, M., & Sekuler, R. (1990). Assimilation and contrast in motion perception: Explorations in cooperativity. *Vision Research, 30*(10), 1439–1451.
Neri, P., Morrone, M. C., & Burr, D. C. (1998). Seeing biological motion. *Nature, 395*(6705), 894–896.
Newsome, W. T., & Pare, E. B. (1988). A selective impairment of motion perception following lesions of the middle temporal visual area (MT). *Journal of Neuroscience, 8*(6), 2201–2211.
Nover, H., Anderson, C. H., & Deangelis, G. C. (2005). A logarithmic, scale-invariant representation of speed in macaque middle temporal area accounts for speed discrimination performance. *Journal of Neuroscience, 25*(43), 10049–10060.
Orban, G. A., & Gulyas, B. (1988). Image segregation by motion: Cortical mechanisms and implementation in neural networks. In R. Eckmiller, & C. van der Malsburg (Eds.), *Neural computers. Series F: Computer and systems sciences* (pp. 149–158).
Orban, G. A., Dupont, P., de Bruyn, B., Vogels, R., & Vandenberghe, R. (1995). A motion area in human visual cortex. *Proceedings of the National Academy of Science USA, Neurobiology, 92*(March), 993–997.
Parrish, E. E., Giaschi, D. E., Boden, C., & Dougherty, R. (2005). The maturation of form and motion perception in school age children. *Vision Research, 45*(7), 827–837.
Peterhans, E., & Von Der Heydt, R. (1989). Mechanisms of contour perception in monkey visual cortex. II. Contours bridging gaps. *Journal of Neuroscience, 9*(5), 1749–1763.
Petkov, N., & Subramanian, E. (2007). Motion detection, noise reduction, texture suppression, and contour enhancement by spatiotemporal Gabor filters with surround inhibition. *Biological Cybernetics, 97*(5–6), 423–439.
Preston, T. J., Li, S., Kourtzi, Z., & Welchman, A. E. (2008). Multivoxel pattern selectivity for perceptually relevant binocular disparities in the human brain. *Journal of Neuroscience, 28*(44), 11315–11327.
Ptito, M., Faubert, J., Gjedde, A., & Kupers, R. (2003). Separate neural pathways for contour and biological-motion cues in motion-defined animal shapes. *NeuroImage, 19*(2), 246–252.
Ptito, M., Kupers, R., Faubert, J., & Gjedde, A. (2001). Cortical representation of inward and outward radial motion in man. *NeuroImage, 14*(6), 1409–1415.
Raudies, F., & Neumann, H. (2010). A neural model of the temporal dynamics of figure–ground segregation in motion perception. *Neural Networks: The Official Journal of the International Neural Network Society, 23*(2), 160–176.
Regan, D. (1989). Orientation discrimination for objects defined by relative motion and objects defined by luminance contrast. *Vision Research, 29*(10), 1389–1400.
Regan, D., & Beverley, K. I. (1984). Figure–ground segregation by motion contrast and by luminance contrast. *Journal of the Optical Society of America A, 1*(5), 433–442.
Regan, D., & Hamstra, S. J. (1992a). Shape discrimination and the judgment of perfect symmetry: Dissociation of shape from size. *Vision Research, 32*(10), 1845–1864.
Regan, D., & Hamstra, S. J. (1992b). Dissociation of orientation discrimination from form detection for motion-defined bars and luminance-defined bars: Effects of dot lifetime and presentation duration. *Spatial Vision, 32*(9), 1655–1666.
Rogers, B., & Graham, M. (1979). Motion parallax as an independent cue for depth-perception. *Perception, 8*(2), 125–134.
Sakai, K., & Nishimura, H. (2006). Surrounding suppression and facilitation in the determination of border ownership. *Journal of Cognitive Neuroscience, 18*(4), 562–579.
Sary, G., Vogels, R., & Orban, G. A. (1993). Cue-invariant shape selectivity of macaque inferior temporal neurons. *Science, 260*, 995–997.
Schrauf, M., Wist, E. R., & Ehrenstein, W. H. (1999). Development of dynamic vision based on motion contrast. *Experimental Brain Research, 124*, 469–473.
Segaert, K., Nygård, G. E., & Wagemans, J. (2009). Identification of everyday objects on the basis of kinetic contours. *Vision Research, 49*(4), 417–428.
Sekuler, A. (1990). Motion segregation from speed differences: Evidence for nonlinear processing. *Vision Research, 30*(5), 785–795.
Shadlen, M. N., Britten, K. H., Newsome, W. T., & Movshon, J. A. (1996). A computational analysis of the relationship between neuronal and behavioral responses to visual motion. *Journal of Neuroscience, 16*(4), 1486–1510.
Shapley, R., & Tolhurst, D. (1973). Edge detectors in human vision. *Journal of Physiology, 229*, 165–183.
Shen, Z., Xu, W., & Li, C. (2007). Cue-invariant detection of centre–surround discontinuity by V1 neurons in awake macaque monkey. *Journal of Physiology, 583*(2), 581–592.
Shulman, G. L., Schwarz, J., Miezin, F. M., & Petersen, S. E. (1998). Effect of motion contrast on human cortical responses to moving stimuli. *Journal of Neurophysiology, 79*(5), 2794–2803.
Siegel, R., & Anderson, R. (1988). Perception of three-dimensional structure from motion in monkey and man. *Nature, 331*, 259–261.
Sillito, A. M., Grieve, K. L., Jones, H. E., Cudeiro, J., & Davis, J. (1995). Visual cortical mechanisms detecting focal orientation discontinuities. *Nature, 378*, 492–496.
Smith, A. T., Greenlee, M. W., Singh, K. D., Kraemer, F. M., & Hennig, J. (1998). The processing of first- and second-order motion in human visual cortex assessed by functional magnetic resonance imaging (fMRI). *Journal of Neuroscience, 18*(10), 3816–3830.
Snowden, R. J., Treue, S., Erickson, R. G., & Andersen, R. A. (1991). The response of area MT and V1 neurons to transparent motion. *Journal of Neuroscience, 11*(9), 2768–2785.
Stanley, D. A., & Rubin, N. (2003). FMRI activation in response to illusory contours and salient regions in the human lateral occipital complex. *Neuron, 37*(2), 323–331.
Stoner, G. R., & Albright, T. D. (1992). Motion coherency rules are form-cue invariant. *Vision Research, 32*(3), 465–475.
Tanaka, K., Hikosaka, K., Hide-aki, S., Yukie, M., Fukada, Y., & Iwai, E. (1986). *Journal of Neuroscience, 6*(1), 134–144.
Tanaka, K., & Saito, H. (1989). Analysis of motion of the visual field by direction, expansion/contraction, and rotation cells clustered in the dorsal part of the medial superior temporal area of the macaque monkey. *Journal of Neurophysiology, 62*(3), 626–641.
Todd, J. (1984). The perception of three-dimensional structure from rigid and non-rigid motion. *Perception and Psychophysics, 36*(2), 97–103.
Tyler, C., Likova, L., Kontsevich, L., & Wade, A. (2006). Cortical area KO is specialized for depth structure. *Cortex, 2*(1), 228–238.
Ullman, S. (1979). The interpretation of structure from motion. *Proceedings of the Royal Society of London Series B – Biological Science, 203*(1153), 405–426.
Van Oostende, S., Sunaert, S., van Hecke, P., Marchal, G., & Orban, G. (1997). The kinetic occipital (KO) region in man: An fMRI study. *Cerebral Cortex, 7*(7), 690–701.
Versavel, M., Orban, G. A., & Lagae, L. (1990). The responses of visual cortical neurons to curved stimuli and chevrons. *Vision Research, 30*(2), 235–248.
Victor, J. D., & Mast, J. (1991). A new statistic for steady-state evoked potentials. *Electroencephalography and Clinical Neurophysiology, 78*(5), 378–388.
Vinberg, J., & Grill-Spector, K. (2008). Representation of shapes, edges, and surfaces across multiple cues in the human visual cortex. *Journal of Neurophysiology, 99*(3), 1380–1393.
Von Der Heydt, R., & Peterhans, E. (1989). Mechanisms of contour perception in monkey visual cortex. I. Lines of pattern discontinuity. *Journal of Neuroscience, 9*(5), 1731–1748.
Wahba, G. (1990). Spline models for observational data. In *CBMS: NSF regional conference series in applied mathematics, 59*. Philadelphia, PA: Society for Industrial and Applied Mathematics.
Wallach, H., & O'Connell, D. (1953). The kinetic depth effect. *Journal of Experimental Psychology, 45*(4), 205–217.
Wattam-Bell, J., Birtles, D., Nyström, P., von Hofsten, C., Rosander, K., Anker, S., et al. (2010). Reorganization of global form and motion processing during human visual development. *Current Biology, 20*(5), 411–415.
Xiao, D. K., Marcar, V. L., Raiguel, S. E., & Orban, G. A. (1997a). Selectivity of macaque MT/V5 neurons for surface orientation in depth specified by motion. *European Journal of Neuroscience, 9*(5), 956–964.
Xiao, D. K., Raiguel, S., Marcar, V., & Orban, G. A. (1997b). The spatial distribution of the antagonistic surround of MT/V5 neurons. *Cerebral Cortex, 7*(7), 662–677.
Zeki, S., Perry, R. J., & Bartels, A. (2003). The processing of kinetic contours in the brain. *Cerebral Cortex, 13*(2), 189–202.